Atmospheric Environment 78 (2013) 154–162

Contents lists available at SciVerse ScienceDirect

Atmospheric Environment

journal homepage: www.elsevier.com/locate/atmosenv

Dynamic variations of ultrafine, fine and coarse particles at the Lu-Lin background site in East Asia

Sheng-Chieh Chen [a,f], Shih-Chieh Hsu [b], Chuen-Jinn Tsai [a,*], Charles C.-K. Chou [b], Neng-Huei Lin [c], Chung-Te Lee [d], Gwo-Dong Roam [e], David Y.H. Pui [f]

[a] Institute of Environmental Engineering, Nation Chiaotung University, Hsinchu 300, Taiwan
[b] Research Center for Environmental Changes, Academia Sinica, Taipei 115, Taiwan
[c] Department of Atmospheric Sciences, National Central University, Jhongli 320, Taiwan
[d] Institute of Environmental Engineering, National Central University, Jhongli 320, Taiwan
[e] National Institute of Environmental Analysis, Environmental Protection Administration, Jhongli 320, Taiwan
[f] Particle Technology Laboratory, Mechanical Engineering, University of Minnesota, Minneapolis, MN 55455, USA

HIGHLIGHTS

- Atmospheric $PM_{0.1}$, $PM_{2.5}$ and PM_{10} were studied at a background site.
- The concentration of biomass burning (BB) makers, K and Mn, elevated significantly.
- Free troposphere around Taiwan is impacted by BB plumes from Southeast Asia.

ARTICLE INFO

Article history:
Received 3 January 2012
Received in revised form
8 May 2012
Accepted 12 May 2012

Keywords:
Atmospheric aerosol
Ultrafine particle
Biomass burning
Biogenic aerosol
Chemical mass closure
Eastward transport

ABSTRACT

The characteristics of atmospheric ultrafine particles (i.e. <100 nm, nanoparticles or $PM_{0.1}$), $PM_{2.5}$ and PM_{10} were studied at the Lulin Atmospheric Background Station (LABS, 2862 m a.s.l., Taiwan) as part of the 7SEAS/Dongsha campaign. Sampling was conducted in July and August of 2009 and September to November of 2010, during which two 96-h and four 72-h PM samples were taken. Real-time particle size distributions were measured continuously from July to August of 2009 and July to November of 2010. $PM_{0.1}$, $PM_{2.5}$ and PM_{10} were collected by using two MOUDIs (micro-orifice uniform deposit impactor, MSP 110) and a Dichotomous PM_{10} sampler (Andersen SA-241) while real-time size distributions of particles of 5.5–350 nm in diameter were measured by an SMPS (scanning mobility particle sizer, TSI 3936). Filter samples were analyzed for gravimetric mass and chemical compositions, including organic carbon (OC), element carbon (EC), water-soluble ions and trace elements. Meteorology parameters and gaseous O_3 and CO concentrations were also monitored along with the SMPS data for studying particle nucleation, condensation, SOA (secondary organic aerosol) formation and long-range air pollutant transport at the LABS. SMPS data showed that nanoparticle concentrations at the LABS remained relatively stable at low level (~300–500 #/cm^3) during the nighttime (22:00–04:00), increased during daytime, and reached a maximum (~2000–4000 #/cm^3) in the afternoon (12:00–16:00). The NMD (number median diameter) showed an opposite trend with the peak number concentrations observed in the afternoon corresponding to the smallest NMD (20–40 nm). These results indicate the dominance of local sources rather than the transport from other atmospheric air because that the lifetime of nanoparticles was only few minutes. Chemical analysis of filter samples showed that the concentrations of trace elements K and Mn, which serve as biomass burning markers, were elevated in the fine particle fractions during November 9–12th when the air mass passed through South and Southeast Asia prior to reaching the LABS. The concentrations of K and Mn would have been low if the aerosols had local origins The biomass burning derived K was found in all fine particle samples at the LABS suggesting that the free troposphere around Taiwan is frequently impacted by the long-range transport of biomass burning plumes via the westerly winds.

* Corresponding author. Tel.: +886 3 573 1880; fax: +886 3 572 7835.
E-mail address: cjtsai@mail.nctu.edu.tw (C.-J. Tsai).

1352-2310/$ – see front matter © 2012 Elsevier Ltd. All rights reserved.
http://dx.doi.org/10.1016/j.atmosenv.2012.05.029

1. Introduction

Atmospheric fine and ultrafine particles are largely contributed by the burning of fuels (fossil fuels and biofuels used in power plants, industry and motor vehicles), forest fire and crop residue burning (the so-called biomass burning, any deliberate burning of agricultural residues for land clearing and land-use change). Particle emissions due to the burning of fuel may not be well controlled due to weak regulations (Li et al., 2011a,b) while those from the burning of biomass are completely unregulated. These combustion particles may act as the cloud condensation nuclei (CCN) responsible for the "cloud-climate" effect and, locally, could be hazardous to public health (Hsu et al., 2009; Kavouras et al., 1998; Li et al., 2011a,b). Scientists have estimated that humans are responsible for about 90% of biomass burning with only a small percentage of natural fires contributing to the total amount of vegetation burned (http://earthobservatory.nasa.gov/Features/BiomassBurning/). Streets et al. (2003) estimated that the annual total amount of biomass burned in South and Southeast Asian countries including China, India and Indo-China peninsula countries was about 500 Tg which was comparable to the total annual biofuel burned in this area, 1300 Tg. In addition to biomass burning, the industrialization of East China has also contributed massive quantities of anthropogenic pollutants into the troposphere and influenced the air quality of East Asian countries (Hsu et al., 2009; Li et al., 2011a,b).

Taiwan is located on the edge of the western Pacific Ocean and adjacent to the Southeast and South Asian countries. The southwest monsoon prevails in summer in Taiwan, whereas the northeast monsoon prevails between fall and spring. At higher elevations around Taiwan the westerlies, wind originating from the Mediterranean Sea and Northern Africa which then passes through the south of Tibet Plateau, prevail at most the time, except in summer. After entering China the westerlies bring moist air to Southern China and Indochina Peninsula. Because of geographical location and meteorological conditions, it has been demonstrated that the air quality of Taiwan can be influenced by South and Southeast Asian biomass burning and industrial and power plant emissions from East China (Andrews et al., 2011; Hsu et al., 2009; Lee et al., 2011; Li et al., 2011a,b; Lin et al., 2009; Ou Yang et al., 2012; Sheu et al., 2010; Wai et al., 2008).

In order to understand the long-term free atmospheric Hg produced by biomass burning from South and Southeast Asian countries, Sheu et al. (2010) measured the gaseous elemental mercury, reactive gaseous mercury and particulate mercury at a high alpine site in Taiwan, the Lulin Atmospheric Background Station (LABS, 2862 m a.s.l.). Because of its elevation, the local anthropogenic pollution can only weakly influence the LABS thus allowing one to differentiate pollutants from long-range transport (Cozic et al., 2008). They concluded that sampled Hg at the LABS might be attributed to the biomass burning of Southeast Asia. Yet, there was still no direct evidence that could demonstrate the collected Hg was from biomass burning. In a recent study biosmoke pollutants from East China, including those originating from biomass burning, were found to raise atmospheric K, Mn, Pb and As concentrations, which have been designated to be good Asian biosmoke markers, in the fine particles of Taiwan (Hsu et al., 2009). Therefore, by conducting size resolved chemical concentration measurements for particles in LABS more direct information of South and Southeast Asian biomass burning as well as the regional pollution from China may be obtained.

Because of the unique location of Taiwan and the high elevation of the LABS, it is worthwhile to conduct a comprehensive measurement of both particles and gaseous pollutants in the LABS. For particle measurement, size-resolved sampling and further chemical analysis was conducted. Meteorological and gaseous pollutants data obtained from the LABS were used to correlate the size distributions of ultrafine particles to potential sources. In addition, back-trajectories of the air masses reaching the LABS were analyzed to correlate the characteristics of PMs sampled at LABS. The results of this study could help in the development of a long-range pollutant transport model and in the establishment of control methods by the Taiwan government.

2. Experimental methods

2.1. Site descriptions

The field study was conducted at the LABS (23°28′07″N, 120°52′25″E), which is a two-story building on the summit of Mt. Front Lulin in Yu-Shan National Park in central Taiwan as shown in Fig. 1. This station was established by Taiwan EPA in 2006 for complementing the global network of Global Atmospheric Watch (GAW) in the East Asia region, where no high-elevation baseline station was available before the appearance of the LABS.

The Tsuga and Picea coniferous forests dominate the surrounding area of the site. In a conifer forest, aerosols can be produced directly from the conifer leaves (epicuticular wax) or indirectly through photooxidization and gas-to-particle conversion. These organic particles, the so-called SOA (secondary organic aerosol), may act as cloud condensation nuclei (Kavouras et al., 1998, 1999). Thus, biogenic aerosols may be produced in the vicinity of the station. Hiking is the only way to access the summit and the nearest main road, which has a very low traffic, is about 2 km (perpendicular distance) away from the LABS. In any case, the existing flourishing forest sheltered the LABS from the pollutants emitted by vehicles. Therefore, the local motor emissions were neglected in this study.

2.2. Sampling protocol

In this study, PM sampling was conducted in July and August of 2009 and September to November of 2010, during which two 96-h and four 72-h PM samples were taken. Real-time particle size distributions were measured continuously from July to August of 2009 and July to November of 2010, except when sporadic shutdown of power occurred. PM samples were collected by two 10-stage MOUDIs (Model 110, MSP Corp., MN, USA) and a Dichotomous PM_{10} sampler (Dichot, Model SA-241, Andersen Inc., Georgia, USA) operated in parallel. In the MOUDIs, the 3.2 μm cutsize stages were replaced with 2.5 μm cutsize stages and the nozzle plates of stage 10 with 56 nm cutsize were removed. Thus, the cutsizes of the MOUDIs were 18, 10, 5.6, 2.5, 1.8, 1.0, 0.56, 0.32, 0.18, and 0.1 μm. That is, the after filters sampled particles smaller than 100 nm ($PM_{0.1}$). Because pressure and temperature at the LABS, which averaged about 0.7 atm and 10 °C, were low the actual operational flow rates of the samplers were adjusted based on the ambient conditions while the concentrations of PMs were calculated based on the standard condition of 25 °C and 1 atm. The $PM_{2.5}$ and PM_{10} concentrations were calculated based on the mass distributions of MOUDI and the collection efficiency curves of the EPA $PM_{2.5}$ Well Impactor Ninety-Six (Peters et al., 2001) and the Hi-Vol Sampler (McFarland et al., 1984), respectively. The Dichot was used to collect $PM_{2.5-10}$ and $PM_{2.5}$ samples. An SMPS (Model 3936, TSI Inc., MN, USA) equipped with a Nano- or Long-DMA (TSI Model 3085 or 3081) and an Ultrafine Condensation Particle Counter (UCPC, TSI Model 3776) was used to measure the size distribution of particles from 8.5 to 350 nm with the Long-DMA or, alternatively, 5.5–210 nm with the Nano-DMA.

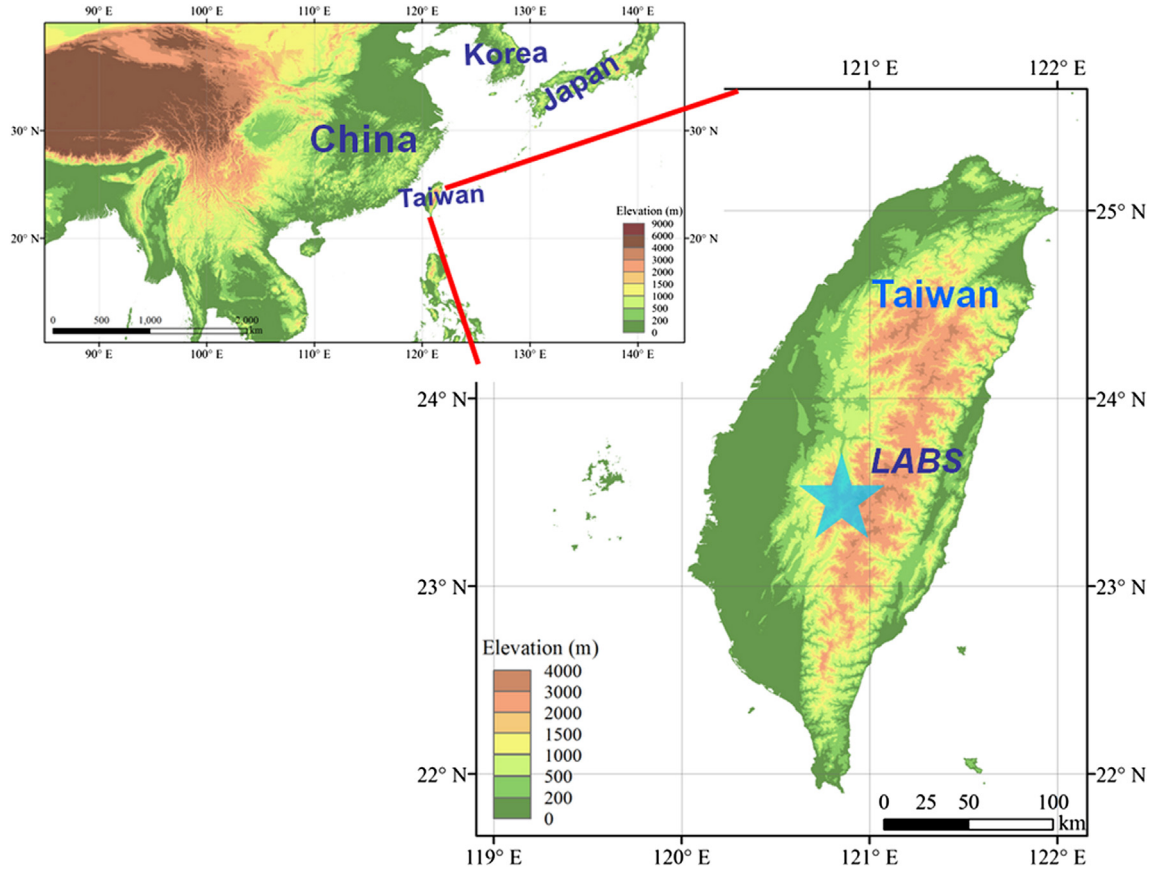

Fig. 1. Location of Taiwan and the Lulin Atmospheric Background Station (LABS).

In the first MOUDI (M1) silicone grease coated aluminum foil was used as the impaction substrate in 0–9 stages to reduce solid particle bounce (Chen et al., 2011) and 2 quartz filters (Tissuquartz 2500QAT-UP, 7201 & 7202, Pall Corp., New York, USA) in series were used as the after filters for ultrafine particle OC and EC sampling (QBQ method). In the second MOUDI (M2), Teflon filters (TefloR2PL047, Pall Corp., New York, USA) were used in every stage and in the after filter. In the Dichot, quartz filters were used in the both fine and coarse particle channels (QBQ method). In every sampling run, at least two Teflon filters, two quartz filters and two uncoated and grease coated Aluminum foils were used as laboratory and field blanks for gravimetric or chemical analysis.

Meteorological parameters at the LABS, including temperature, relative humidity, solar radiation, wind direction and wind speed, were measured continuously by various research groups (Lee et al., 2011; Ou Yang et al., 2012; Sheu et al., 2010) and were used in the current study. In addition, gaseous pollutant data monitored at the station, such as O_3 and CO, were also used to help elucidate the current experimental data.

2.3. Sample analysis

A detailed description of the sample analyses can be found elsewhere (Chen et al., 2010) and is described briefly in the following. All aluminum foil and Teflon filter PM samples were analyzed gravimetrically by a microbalance (Model CP2P-F, Sartorius, Germany). Further chemical analysis was conducted for the Teflon (water soluble ions and elements) and quartz (OC and EC) samples. Before weighing, filters were conditioned at least 24-h in a temperature and relative humidity controlled room (22 ± 1 °C, 40 ± 3% RH). The PM mass of each stage, 0–9, of M1 and M2 was compared to each other to examine whether particle bounce occurred in M2, using M1 as the reference MOUDI (Chen et al., 2011). After gravimetric analysis, the Teflon filter was cut into equal halves using a Teflon coated scissors. One half was analyzed by ICP-MS (Elan 6100, PerkinElmer, Waltham, Massachusetts, USA) for elements while the other half was analyzed by ion chromatography (IC, Model DX-120, Dionex Corp, Sunnyvale, CA) for water soluble ionic species. The quartz filter samples of the M1 ($PM_{0.1}$) and Dichot ($PM_{2.5}$ and $PM_{2.5-10}$) were analyzed by the thermal-optical reflectance (TOR) method for OC and EC concentrations. In accordance with Turpin and Lim (2001), Kavouras et al. (1999) and Kavouras and Stephanou (2002), the POM (particulate organic mass) to POC (particulate organic carbon) ratio at LABS was assumed to be 1.4 for all PMs size fractions since pinic acid and pinonic acid (both belong to carboxylic acids which contain less organic oxygen) were the dominant organic compounds in the conifer forest. In order to correlate the aerosol collected at the LABS to biomass burning emission from South and Southeast Asian countries and other sources, air mass back-trajectory analysis was conducted using the NOAA HYSPLIT model.

3. Results and discussion

3.1. PM concentration and mass distribution

The gravimetric analysis of all laboratory and field blanks showed that the weight differences between pre- and post-sampling were less than 1 μg, which was much lower than the lowest $PM_{0.1}$ mass in this study. In addition, particles collected in each impaction stage always had a higher mass than that at the after filter ($PM_{0.1}$). Therefore, the data of the gravimetric analysis in this study were reliable.

Throughout the majority of the sampling campaign, a close agreement between PM mass collected on the same stages of M1 and M2 was observed in all samples, with relative differences being <10%, due to the relatively high RH at the LABS which significantly reduced solid particle bounce. However, during Nov. 9th ~ Nov. 12th, lower RH of less than 65% persisted for about 40 h during the 72-h sampling, resulting in a slightly larger difference between M1 and M2. Nevertheless, the maximum difference was only 15%, which occurred at stage 3 ($PM_{2.5-5.6}$), indicating that the effect of solid particle bounce in M2 could be neglected in this study.

Table 1 summarizes the sampling date, start/end time, weather condition and the corresponding PM_{10}, $PM_{2.5}$ and $PM_{0.1}$ concentrations of the six samples. The $PM_{0.1}$ was 0.08–0.2 μg m^{-3} at the LABS, much lower than that in urban areas (1–3 μg m^{-3}, Chen et al., 2010). Low $PM_{0.1}$ concentrations, 0.08 μg m^{-3}, as well as relatively low PM_{10} and $PM_{2.5}$ concentrations were observed in samples (b) and (e), which was due to precipitation scavenging. For the samples taken in sunny days (samples a, c, d and f), the average concentrations of PM_{10}, $PM_{2.5}$ and $PM_{0.1}$ were 7.18, 5.46 and 0.15 μg m^{-3}, respectively. The average PM_{10} concentration of the four sunny measurements was very close to that measured by the R&P TEOM 1400a (Rupprecht & Patashnick Co., Inc., East Greenbush, NY, USA) of the LABS, which was 8.14 μg m^{-3}, demonstrating that the PM_{10} was accurately sampled by the MOUDIs. However, the current PM_{10} concentration was slightly higher than that observed at a similar high alpine site (Jungfraujoch) in Cozic et al. (2008), which was only 4.5 μg m^{-3}. This could be attributed to the fact that the LABS received more long-range transport pollutants than Jungfraujoch.

Fig. 2 compares the mass distributions of samples (a), (c), (e) and (f) which represent the distributions obtained on sunny days in summer (sample a), rainy days in fall (sample e) and sunny days in fall (samples c and f), respectively. Distributions of samples (b) and (d) are not shown because they have similar distributions to those of samples (e) and (c), respectively. On sunny days, distributions from samples (a), (c) and (f) all have a single mode with a MMAD (mass median aerodynamic diameter) close to 1 μm. The general-unimodal distribution observed at LABS was in agreement with that was found by Leaitch and Isaac (1991) who attributed this to the precipitation scavenging and deposition of smaller and larger particles in the middle troposphere above the clouds. Although the size distribution of sample (c) demonstrated a good fit with a single mode, a slight increase in the concentrations of both coarse and fine particle fractions was observed. This was attributed to the LABS receiving aged maritime airs from the Pacific Ocean (chemical data will be shown later). In contrast, the distributions obtained on rainy days had both accumulation and coarse modes (samples b and e). This was because fine particles contained inorganic salts, underwent deliquesce under high RH and grew in size.

3.2. Size distribution of ultrafine particles

Based on the SMPS data, this study found that the size distribution of ultrafine particles at LABS varied dramatically with time

Table 1
PM concentrations (μg m^{-3}) of all six samples.

Sample	Date	Start/end time	Weather	PM_{10}	$PM_{2.5}$	$PM_{0.1}$
(a)	July 6th–9th, 2009	18:00	Sunny	8.33	6.17	0.20
(b)	Aug. 4th–8th, 2009	18:00	Rainy	2.36	1.44	0.08
(c)	Sep. 29th–Oct. 2nd, 2010	12:00	Sunny	7.87	5.86	0.11
(d)	Oct. 2nd–Oct. 5th, 2010	13:00	Sunny	6.38	4.91	0.12
(e)	Nov. 5th–Nov. 9th, 2010	16:00	Rainy	2.21	1.55	0.08
(f)	Nov. 9th–Nov. 12th, 2010	17:00	Sunny	6.12	4.90	0.18

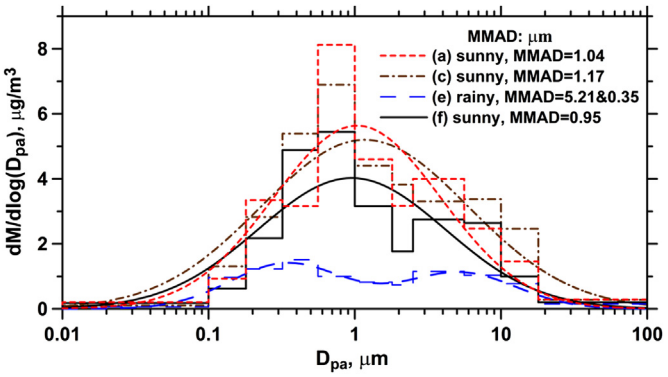

Fig. 2. Comparison of mass distributions sampled on a sunny day in summer (a), rainy day in fall (e) and sunny day in fall (f).

and was a function of various factors, including atmospheric air mass, temperature, RH, solar radiation, wind direction and speed, O_3 concentration, etc. However, a quantitative evaluation of the relative importance of these factors is not possible at present. Fig. 3 represents three typical size distributions observed at the LABS, which were obtained in the sunny daytime (thick line) and nighttime (thin line) at LABS on July 7th and August 24th of 2009 and Nov. 11th of 2010.

The three daytime distributions all show a nuclei mode at about 15 nm. Because the lifetime of these small particles is very short (normally on the order of minutes), the data suggest the existence of a local source. The nuclei mode particles can be produced only by combustion or via homogeneous or heterogeneous gas-to-particle conversion. However, no combustion event occurred in the vicinity of the sampling site. Thus, the nanoparticles could only be attributed to in-situ formation via gas-to-particle conversion from biogenic emissions. The differences in the peak concentrations of the nuclei modes between the daytime distributions were mainly due to the varying intensities of the photochemical reaction and the wind speed which affects dilution. An obviously higher O_3 consumption (O_3 concentration 19 → 10 ppb in 3 h) and lower wind speed (<1 m s^{-1}) was observed on Aug. 24th relative to that observed on the other two days. Higher consumption of O_3 would enrich the formation of organic acid particles (Kavouras et al., 1999; Kavouras and Stephanou, 2002) and the weaker dilution effect facilitated the accumulation of newly formed particles, explaining the much higher $PM_{0.1}$ concentration on Aug. 24th. The distribution

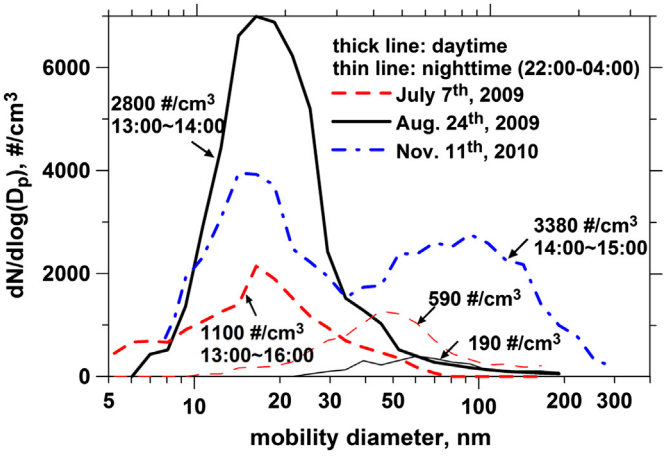

Fig. 3. Typical size distributions and total number concentrations of ultrafine particles at the LABS.

of Nov. 11th (14:00–15:00) represented a special case when both nucleation and accumulation modes (peaks at ~15 and ~100 nm, respectively) existed simultaneously. This was due to a dramatic increase of RH (50 → 80%) and a reduced temperature (14 → 10 °C) which, due to the condensation effect, enriched the accumulation mode (100–300 nm) with water droplets and other organic vapors (Kavouras et al., 1999).

The particle number distribution of the July 7th, which represents a case typical for the afternoon (13:00–16:00) of sunny days, had an average total $PM_{0.1}$ concentration of ~1000 #/cm^3. In comparison, the particle number concentration was relatively lower at nighttime than that at daytime. On average, the concentration was only ~500 #/cm^3. Moreover, a lower than typical $PM_{0.1}$ concentration of <200 #/cm^3 was observed on the nighttime of Aug. 24th when it rained.

Fig. 4 shows the general time series of the number concentration of $PM_{0.1}$, NMD (number median diameter), temperature, RH, O_3 concentration and solar radiation flux during Sep. 29th to Oct. 2nd, 2010. It is seen that the $PM_{0.1}$ concentration, temperature and solar intensity peaked at around noon while the O_3 concentration, RH and NMD was at a minimum near the noon. The noon peak concentration of $PM_{0.1}$ was 1000–1500 #/cm^3 and it was reduced to 200–500 #/cm^3 near midnight. The NMD was reduced to 20–40 nm near noon while it was increased with the increasing RH to 80–100 nm near midnight. That is, the $PM_{0.1}$ concentration increased with the increasing temperature and solar intensity, but NMD and O_3 showed a reverse trend. The observation of a reduced O_3 concentration at the daytime (6 am–6 pm), also seen by Ou Yang et al. (2012) at the LABS, demonstrates that high solar radiation promoted a photo-oxidative reaction which produced the SOAs (secondary organic aerosols) at the LABS.

Other than the typical particle distribution and meteorological data shown in Fig. 4, an unusually high CO concentration coinciding with a dramatic decrease of RH was observed and is presented in Fig. 5. It can be seen the CO concentration was as high as 220 ppb in the evening of Nov. 9th, which was about two times the annual average concentration of ~130 ppb measured at the LABS in 2010 (data were not published). Accompanying the high CO concentration was a dramatic variation of RH, which increased to 100% then very quickly reduced to as low as 10%. This was due to the subsidence of the upper tropospheric air characterized by a low RH. That is, the LABS could receive air pollutants transported from the upper free troposphere. In Fig. 5, it is seen that the number concentrations of $PM_{0.1}$ increased with increasing RH, which was different from

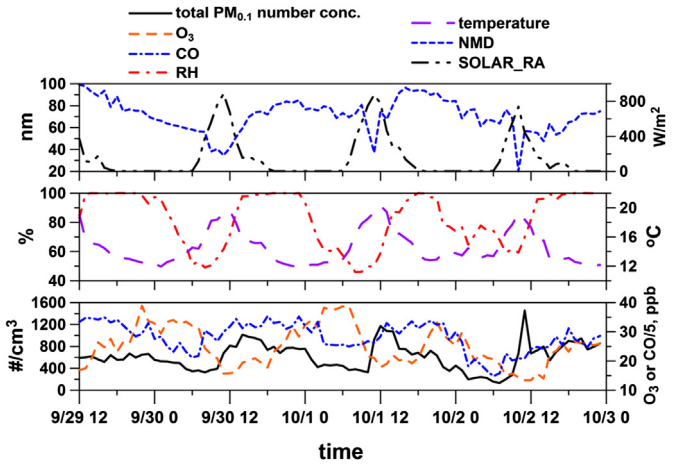

Fig. 4. A typical time series of the $PM_{0.1}$ number concentration and NMD (number median diameter) along with temperature, RH, O_3 concentration and solar radiation for Sep. 29th–Oct. 3rd, 2010.

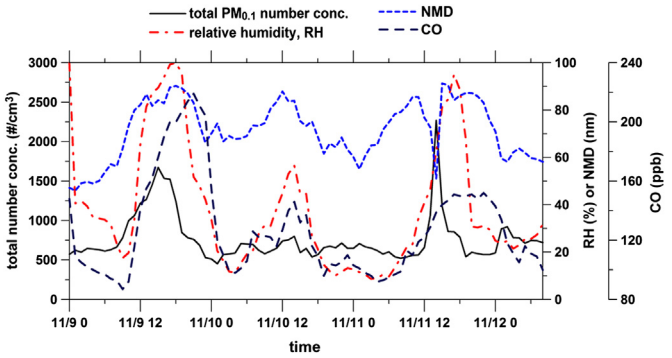

Fig. 5. Time series of the number concentration of $PM_{0.1}$, NMD, RH and CO concentration when the upper tropospheric air mass descended to LABS.

that observed in Fig. 4. This unusual distribution can be found in Fig. 3 (14:00–15:00 of Nov. 11th). Moreover, the lowest NMD in this time period was found to be relatively large (~60 nm, condensation effect). It is to be noted again, the current ultrafine particles basically were SOA and generated from local biogenic source mainly.

3.3. Chemical compositions of PMs

Based on the QBQ method, this study found the average OC positive artifact to be 240 ± 90% for $PM_{0.1}$, 18.6 ± 12.7% for $PM_{2.5}$, and 13.4 ± 9.3% in the PM_{10}. Higher artifact was found in $PM_{0.1}$ and on rainy days when PM mass was low.

Accounting for the correction of the positive artifact, Table 2 shows the comparison of the chemical compositions (%) including OM, EC, ions and elements for $PM_{0.1}$, $PM_{2.5}$ and PM_{10} between the six experimental campaigns at the LABS. It can be seen that a good chemical mass closure (OM + EC + ions + elements) was obtained for all PMs, where $PM_{0.1}$ was 70.7–85.6%, $PM_{2.5}$ was 54.8–73.5% and PM_{10} was 59–75.6%. The lower mass closure in $PM_{2.5}$ and PM_{10} could be attributed to a relatively lower OM content. The use of the OM/OC ratio of 1.4 for $PM_{2.5}$ and PM_{10} may underestimate the OM concentration because the fine and coarse particles collected in LABS could contain a certain amount of atmospheric aged aerosols which were designated as high polarity, water soluble organic acids. The OM/OC ratio was found to be 1.8 in Cozic et al. (2008). After adopting 1.8 for the OM/OC ratio, the present mass closure would increase by 11–21% for both $PM_{2.5}$ and PM_{10}.

For July 6–9th (sample a), OM and EC data are not shown because the quartz filter samples were not taken. In this sample, water soluble ions contributed 5.3, 12.2 and 11.4% and elements contributed 0.02, 7.3 and 10.1% to $PM_{0.1}$, $PM_{2.5}$ and PM_{10}, respectively. From the air mass back-trajectory analysis, it was found that before reaching the LABS the air passed through the Southeast Provinces of China, where were highly polluted industrial areas. Therefore, the polluted air impacted the LABS and significantly elevated the concentration of elements in $PM_{2.5}$ and PM_{10}. This finding is in agreement with which was observed on Mt. Tai (Li et al., 2011a,b). The anthropogenic pollutants were sampled when the air mass passed through industrial areas before reaching the sampling site.

On the rainy days of Aug. 4–8th (sample b) and Nov. 5–9th (sample e), OM was the most abundant constituent of the PMs. This reflected that the local biogenic source was the most predominate of the LABS particles and that most of the atmospheric particles were scavenged by rain. Unusually high EC content was observed in $PM_{0.1}$ on Nov. 5–9th and in $PM_{2.5}$ and PM_{10} on Aug. 4–8th, which might be due to the relatively low wet scavenging efficiency for EC.

Table 2
Chemical composition (%) of $PM_{0.1}$, $PM_{2.5}$ and PM_{10} at LABS.

LABS	Sample	PM ($\mu g\ m^{-3}$)	OM %	EC %	Ions %	Elements %	Total %
$PM_{0.1}$	(a)	0.20	–[a]	–	5.3	0.02	–
	(b)	0.08	70.0	7.3	5.1	1.3	83.7
	(c)	0.11	55.6	14.0	8.1	2.5	80.2
	(d)	0.12	46.7	10.8	11.5	1.7	70.7
	(e)	0.08	54.4	17.0	9.0	2.2	82.6
	(f)	0.18	61.8	5.4	11.4	7.0	85.6
$PM_{2.5}$	(a)	6.17	–	–	12.2	7.3	–
	(b)	1.44	48.0	12.1	5.4	2.5	68.0
	(c)	5.86	28.4	3.5	30.9	2.1	64.9
	(d)	4.55	24.9	5.7	40.9	2.0	73.5
	(e)	1.55	43.2	5.1	4.6	1.9	54.8
	(f)	4.50	31.7	3.4	24.6	5.2	64.9
PM_{10}	(a)	8.33	–	–	11.4	10.1	–
	(b)	2.36	40.0	14.2	4.3	2.1	60.6
	(c)	7.87	26.5	3.3	29.2	2.5	61.5
	(d)	5.79	28.5	4.9	39.5	2.7	75.6
	(e)	2.21	47.4	4.3	5.2	2.1	59.0
	(f)	6.12	35.4	2.9	23.5	6.7	68.5

[a] No data.

On the sunny days, Sep. 29th–Oct. 2nd (sample c) and Oct. 2nd–5th (sample d), OM was the most abundant species in $PM_{0.1}$ while water soluble ions dominated $PM_{2.5}$ and PM_{10}. The above data were in very good agreement with the results of the air mass back-trajectory analysis which showed that the air mass passed over the Pacific Ocean before reaching LABS. Therefore, atmospheric aged aerosols influenced the LABS during the two sampling periods while locally produced SOA still dominated $PM_{0.1}$.

On Nov. 9–12th (sample f), when a high elevation air mass (from trajectory data) influenced the LABS, OM was still the most abundant species in $PM_{0.1}$. It is to be noted that the concentrations of the elements Al, Fe, K, Mn, Ba, Zn, Cu, Pb, Rb etc. were elevated, accounting for 7% of $PM_{0.1}$ mass, which was 4.5 times higher than the average (~1.5%) of other five samples. The results indicated that the downward airflow brought a non-negligible amount of aged nanoparticles enriched in these elements to the LABS. In the $PM_{2.5}$ and PM_{10}, OM was still the most abundant species while ions and elements were elevated. The ions were 24.6 and 23.5% and elements were 5.18 and 6.73% in $PM_{2.5}$ and PM_{10}, respectively.

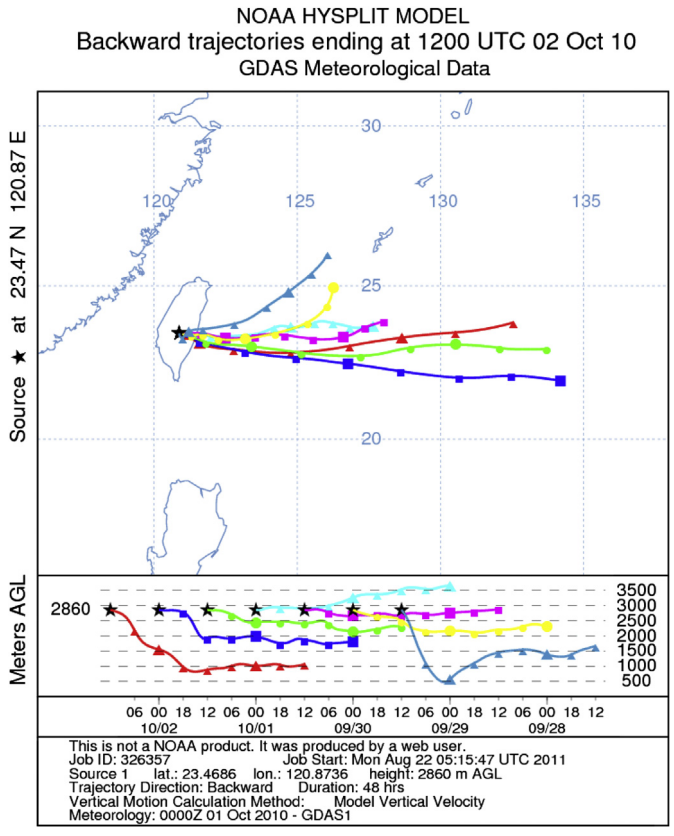

Fig. 6. Air mass back-trajectory analysis during Sep. 29th–Oct. 2nd, 2010 (NOAA HYSPLIT).

3.4. Chemical characteristics of PMs at LABS

Based on the data shown above, it can be concluded that the aerosols present at the LABS had the same origins as those were observed in Cozic et al. (2008). That is, a high alpine site could receive vertically transported aerosols from the boundary layer (in summer) and from the free troposphere (from fall to spring). In addition to the above two sources, locally produced biogenic aerosols, which predominated in ultrafine fraction which predominated in ultrafine fraction, were another important source at the LABS. Thus, the mixing of varying sources resulted in the complex chemical characteristics of PMs at the LABS and it is very

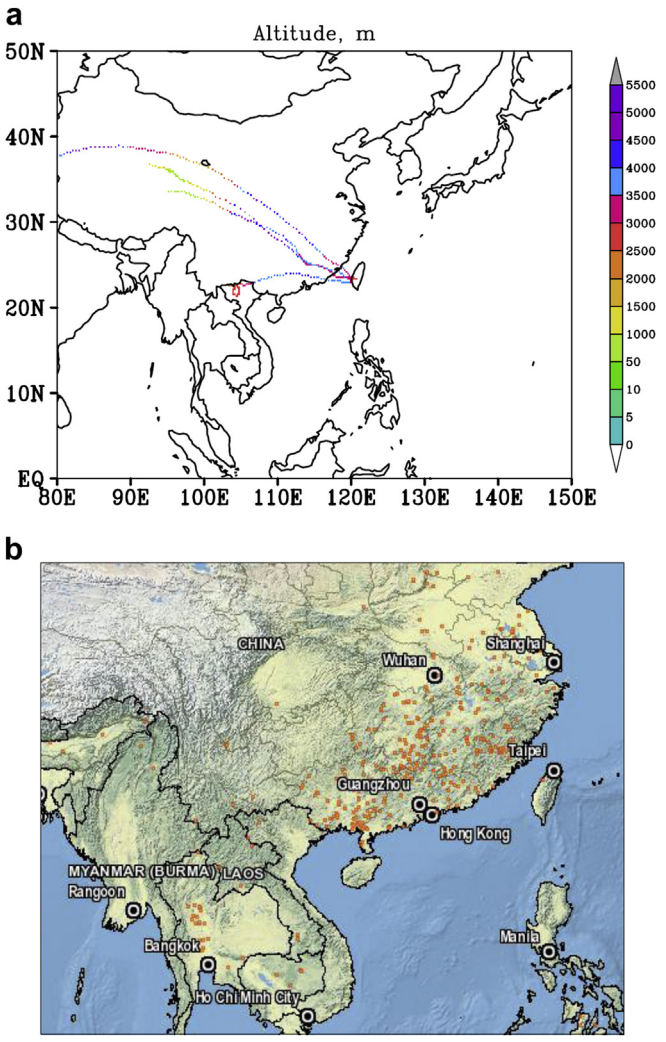

Fig. 7. (a) Five-day air mass backward trajectory analysis and (b) fire events (dots indicate the fire locations retrieved from satellite, based on Fire Information for Resource Management System (FIRMS), http://earthdata.nasa.gov/data/nrt-data/firms during Nov. 9–12th, 2010.

important to understand their contributions for the development of regional and global transport models in the future (Li et al., 2011a,b).

In samples (c) (Sep. 29th–Oct. 2nd) and (d) (Oct. 2nd–5th), a significantly high content of ions in $PM_{2.5}$ and PM_{10} and a moderate content of ions in $PM_{0.1}$ were observed. This finding could be attributed to the origin of air mass. Fig. 6 shows the air trajectories, from the NOAA HYSPLIT Model, of Sep. 29th–Oct 2nd (sample c), in which two-day backward trajectories with an interval of 12-h are presented. The air trajectories of sample (d) were not shown since they were similar to those of sample (c). In Fig. 6, it is seen that the air mass came from the Pacific Ocean. Therefore, LABS received marine aerosols during the sampling periods. Ionic analysis found SO_4^{2-} was the most abundant species in the water soluble ions, which agrees with our previous finding (Lee et al., 2011). SO_4^{2-} contributed ~80% of the total ions in $PM_{2.5}$ for both samples (c) and (d) and ~40 and ~50% in $PM_{2.5-10}$ for samples (c) and (d), respectively. In addition, it was found that coarse particles ($PM_{2.5-10}$) had relatively higher concentrations of Cl^-, Na^+ and K^+ than those of fine particles in the two samples. These findings are in accord with the observation in Fitzgerald (1991) where fine particles in the clean marine air were shown to be composed predominantly of non-sea-salt sulfate whereas sea salt was the most abundant species in coarse particles.

As mentioned earlier, LABS was influenced by a high elevation air mass during Nov. 9–12th (sample f), when the dry and dense air subsided to the LABS. Fig. 7(a) shows the five-day backward trajectories obtained from the NOAA HYSPLIT Model with an interval of 24-h during the sampling period of sample (f) and Fig. 7(b) shows the fire events during these days. It can be seen that the air mass trajectories have a direction similar with the westerlies. In addition, they rose to a high elevation of ~5000–6000 m a.s.l. in the middle China areas and then descended to ~3000–4000 m a.s.l. in the southeast China areas before reaching the LABS. Therefore, it can be concluded that the air mass was driven by the westerlies and then impacted the LABS during the measurement (f). In addition, it can be seen from Fig. 7(b) that southeast China was riddled with fire events, which was helpful in interpreting why the sample (f) contained high concentrations of biomass burning makers, as will be shown later. Furthermore, according to the Fire Information for Resource Management System (FIRMS), it was seen that smoke covered southeast China (data not shown) during the sampling (f).

Fig. 8 depicts the size distributions of K, Mn, Pb and As concentrations for the sample (f) and the average distributions for other samples. All these elements in sample (f) show a bimodal pattern, but the former two elements display a typical distribution with the peak concentrations at 2.5–5.6 μm and around 1 μm. The latter two elements are similar to a unimodal pattern with a pronounced peak at 1 μm and a minor peak in the coarse fraction. The size distribution of K observed in the sample (f) is very similar to that measured in northern Taiwan during the northeastern monsoon when the Asian outflows prevail and has been applied as an indicator of Asian biosmoke aerosols (Hsu et al., 2009). The average distributions of the other samples resembled that of sample (f) except that some distinctive features were found. First, the average distribution seemed to be relatively flat in comparison to sample (f). Second, the average distribution of Mn had the largest peak at the smaller size; while the averaged distribution of potassium peaked at the coarse size. In addition, it was noted that there

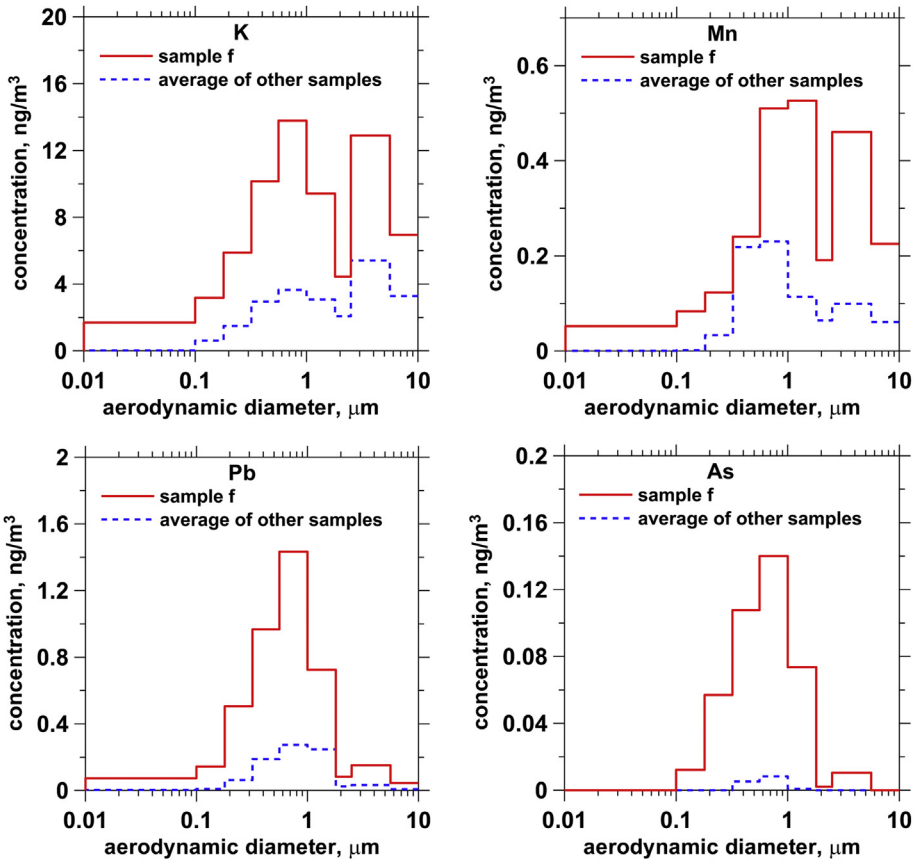

Fig. 8. Comparison of the concentration distributions of biomass burning makers, K, Mn, Pb and As, between Nov. 9–12th, 2010 and the average of the other sampling days.

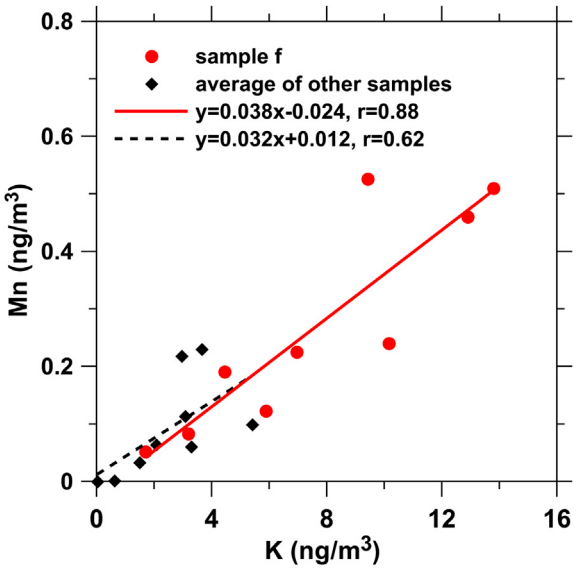

Fig. 9. Comparison of K and Mn concentrations between sample f and samples b–e.

were higher concentrations for these selected metals (K, Mn, Pb and As) in all size fractions of sample (f). Sea salt and mineral dust aerosols were also the significant contributors for aerosol K apart from biomass burning (Andreae, 1983; Park et al., 2007; Hsu et al., 2009). Thus, the size distribution patterns of K can reflect the relative dominance of various sources. For instance, natural sources would preferentially contribute to the coarse fraction while anthropogenic sources would reside in finer sized aerosols (Hsu et al., 2009). Finer particles containing Mn might also be attributable to biomass burning (Viana et al., 2008). Accordingly, we may conclude that particle emissions resulting from biomass burning existed throughout the sampling periods, with the influence being most evident in sample (f). Along with biomass burning, As and Pb in the samples represented the contributions of other anthropogenic sources such as coal burning and industrial emissions (Hsu et al., 2009; Mkoma et al., 2009; Christian et al., 2010).

Fig. 9 shows the correlation between Mn and K mass concentration in sample (f) and the average of samples (b–e). It can be seen the concentrations exhibit a linear correlation. For sample (f) the slope of this line is 0.038 which was much higher than that in the average crust composition (slope of 0.05–0.16) but was close to 0.041–0.045 previously reported in Taipei aerosols, likely serving as a signature of Asian biosmoke particulate pollutants (Hsu et al., 2009). In comparison, the data for samples (b-e) had a smaller slope (or Mn/K ratio) of 0.032. The result suggests that the Mn/K ratio of around 0.04 could serve as a tracer of biomass burning aerosols.

Furthermore, another marker of biomass burning, CO, was observed to be elevated to 220 ppb (Fig. 4) during the Nov. 9–12th measurement (sample f). That is, biomass burning from South and Southeast Asian was able to influence all PMs at the LABS when the westerlies prevailed. Because fine potassium derived from biomass burning was measured throughout all samples, it suggested that the air quality at high mountains over Taiwan, as well as that at ground level, is impacted frequently by biomass burning pollution from the long-range transport by the westerlies.

4. Conclusions

In this study, the average concentration of $PM_{0.1}$, $PM_{2.5}$ and PM_{10} at the LABS were 0.13, 4.0 and 5.4 μg m^{-3}, respectively. In addition to the gravimetric analysis, size resolved chemical compositions including OC, EC, water-soluble ions and trace elements were also determined. Good chemical mass closures for PMs were obtained after taking into account the OC artifact using OM/OC = 1.4 in $PM_{0.1}$ and OM/OC = 1.8 in $PM_{2.5}$ and PM_{10}, which were 80.6 ± 5.9% for $PM_{0.1}$, 81.2 ± 6.8% for $PM_{2.5}$, and 81.0 ± 6.9% for PM_{10}.

The size distributions of ultrafine particles at the LABS were explained with the aid of meteorological data, including temperature, RH, wind speed and direction radiation flux, and gas pollutant concentrations, including CO and O_3 concentrations. It was found that the concentration of ultrafine particles was increased while the NMD decreased with increasing temperature, radiation intensity and O_3 consumption.

Chemical constituents of PMs showed that the aerosol particles at the LABS originated from both on-site biogenic sources and long-range transport. Specifically, the local sources were dominant on rainy days, corresponding to a high OC content in particles when the atmospheric aerosols were scavenged to a large extent. On the sunny days, the two sources were found to be equally important. Backward trajectory analyses in conjunction with the results of chemical analysis were able to interpret the sources well. When the air mass passed over the Pacific Ocean fine particles were predominantly composed of non-sea-salt sulfate, while sea salt was the most abundant species in the coarse particles. In addition, biomass markers K and Mn were found to be elevated in all PM fractions, especially in the fine fraction, when the westerlies prevailed. Because the biomass burning derived fine potassium was measured throughout all samples, it suggests that high elevations (i.e., free troposphere) around Taiwan are perhaps impacted frequently by biomass burning from Southeastern Asia via long-range transport.

Acknowledgement

The financial support of the Taiwan EPA (EPA-98-U1U1-02-103 and EPA-99-U1U1-02–103) is gratefully acknowledged.

References

Andreae, M.O., 1983. Soot carbon and excess fine potassium: long-range transport of combustion-derived aerosols. Science 220, 1148–1151.
Andrews, E., Ogren, J.A., Bonasoni, P., Marinoni, A., Cuevas, E., Rodríguez, S., Sun, J.Y., Jaffe, D.A., Fischer, E.V., Baltensperger, U., Weingartner, E., Collaud Coen, M., Sharma, S., Macdonald, A.M., Leaitch, W.R., Lin, N.-H., Laj, P., Arsov, T., Kalapov, I., Jefferson, A., Sheridan, P., 2011. Climatology of aerosol radiative properties in the free troposphere. Atmospheric Research 102, 365–393.
Chen, S.-C., Tsai, C.-J., Huang, C.-Y., Chen, H.-D., Chen, S.-J., Lin, C.-C., Chou Charles, C.-K., Lung, S.-C., Roam, G.-D., Wu, W.-Y., Smolik, J., Dzumbova, L., 2010. Chemical mass closure and chemical characteristics of ambient $PM_{0.1}$, $PM_{2.5}$ and PM_{10} in a highway tunnel and at a roadside. Aerosol Science Technology 44, 713–723.
Chen, S.-C., Tsai, C.-J., Chen, H.-D., Huang, C.-Y., Roam, G.-D., 2011. The influence of relative humidity on nanoparticle concentration and particle mass distribution measurements by the MOUDI. Aerosol Science Technology 45 (5), 713–723.
Christian, T.J., Yokelson, R.J., Cárdenas, B., Molina, L.T., Engling, G., Hsu, S.-C., 2010. Trace gas and particle emissions from domestic and industrial biofuel use and garbage burning in central Mexico. Atmospheric Chemistry and Physics 10, 565–584.
Cozic, J., Verheggen, B., Weingartner, E., Crosier, J., Bower, K.N., Flynn, M., Coe, H., Henning, S., Steinbacher, M., Henne, S., Coen, M.C., Petzold, A., Baltensperger, U., 2008. Chemical composition of free tropospheric aerosol for PM1 and coarse mode at the high alpine site Jungfraujoch. Atmospheric Chemistry and Physics 8, 407–423.
Fitzgerald, J.W., 1991. Marine aerosols: a review. Atmospheric Environment 25A, 533–545.
Hsu, S.-C., Liu, S.-C., Huang, Y.-T., Chou, C.C.-K., Lung, S.-C.C., Liu, T.-H., Tu, J.-Y., Tsai, F., 2009. Long-range southeastward transport of Asian biosmoke pollution: signature detected by aerosol potassium in Northern Taiwan. Journal of Geophysical Research 114, D14301.
Kavouras, I.G., Mihalopoulos, N., Stephanou, E.G., 1998. Formation of atmospheric particles from organic acids produced by forests. Nature 395, 683–685.
Kavouras, I.G., Mihalopoulos, N., Stephanou, E.G., 1999. Secondary organic aerosol formation vs primary organic aerosol emission: In situ evidence for the

chemical coupling between monoterpene acidic photooxidation products and new particle formation over forests. Environmental Science Technology 33, 1028–1037.

Kavouras, I.G., Stephanou, E.G., 2002. Direct evidence of atmospheric secondary organic aerosol formation in forest atmosphere through heteromolecular nucleation. Environmental Science Technology 36, 5083–5091.

Leaitch, W.R., Isaac, G.A., 1991. Tropospheric aerosol size distributions from 1982 to 1988 over Eastern North America. Atmospheric Environment 25A, 601–619.

Lee, C.-T., Chuang, M.-T., Lin, N.-H., Wang, J.-L., Sheu, G.-R., Chang, S.-C., Wang, S.-H., Huang, H., Chen, H.-W., Liu, Y.-L., Weng, G.-H., Lai, H.-Y., Hsu, S.-P., 2011. The enhancement of PM2.5 mass and water-soluble ions of biosmoke transported from Southeast Asia over the Mountain Lulin site in Taiwan. Atmospheric Environment 45, 5784–5794.

Li, W., Zhou, S., Wang, X., Xu, Z., Yuan, C., Yu, Y., Zhang, Q., Wang, W., 2011a. Integrated evaluation of aerosols from regional brown hazes over northern China in winter: concentrations, sources, transformation, and mixing states. Journal of Geophysical Research 116, D09301. http://dx.doi.org/10.1029/2010JD015099.

Li, W.-J., Zhang, D.-Z., Shao, L.-Y., Zhou, S.-Z., Wang, W.-X., 2011b. Individual particle analysis of aerosols collected under haze and non-haze conditions at a high-elevation mountain site in the North China plain. Atmospheric Chemistry and Physics 8, 407–423.

Lin, C.-Y., Hsu, H.-M., Lee, Y.-H., Kuo, C.-H., Sheng, Y.-F., Chu, D.A., 2009. A new transport mechanism of biomass burning from Indochina as identified by modeling studies. Atmospheric Chemistry and Physics 9, 7901–7911.

Mkoma, S.L., Maenhaut, W., Chi, X., Wang, W., Raes, N., 2009. Characterisation of PM_{10} atmospheric aerosols for the wet season 2005 at two sites in East Africa. Atmospheric Environment 43, 631–639.

McFarland, A.R., Ortiz, C.A., Bertch Jr., R.W., 1984. A 10 mm cutpoint size selective inlet for Hi-Vol Samplers. Journal of the Air Pollution Control Association 34, 544–547.

Ou Yang, C.F., Lin, N.H., Sheu, G.R., Lee, C.T., Wang, J.L., 2012. Seasonal and diurnal variations of ozone at a high-altitude mountain baseline station in East Asia. Atmospheric Environment 46, 279–288. http://dx.doi.org/10.1016/j.atmosenv.2011.09.060.

Park, R.J., Jacob, D.J., Logan, J.A., 2007. Fire and biofuel contributions to annual mean aerosol mass concentrations in the United States. Atmospheric Environment 41, 7389–7400.

Peters, T.M., Vanderpool, R.W., Wiener, R.W., 2001. Design and calibration of the EPA $PM_{2.5}$ Well Impactor Ninety-Six (WINS). Aerosol Science Technology 34, 389–397.

Sheu, G.-R., Lin, N.-H., Wang, J.-L., Lee, C.-T., Ou Yang, C.-F., Wang, S.-H., 2010. Temporal distribution and potential sources of atmospheric mercury measured at a high-elevation background station in Taiwan. Atmospheric Environment 44, 2393–2400.

Streets, D.-G., Yarber, K.-F., Woo, J.-H., Carmichael, G.R., 2003. Biomass burning in Asia: annual and seasonal estimates and atmospheric emissions. Global Biogeochemical Cycles 17, 1099.

Turpin, B.J., Lim, H.J., 2001. Species contributions to $PM_{2.5}$ mass concentrations: revisiting common assumptions for estimating organic mass. Aerosol Science Technology 35, 602–610.

Viana, M., López, J.M., Querol, X., Alastuey, A., García-Gacio, D., Blanco-Heras, G., López-Mahía, P., Piñeiro-Iglesiasc, M., Sanz, M.J., Sanz, F., Chi, X., Maenhaut, W., 2008. Tracers and impact of open burning of rice straw residues on PM in Eastern Spain. Atmospheric Environment 42, 1941–1957.

Wai, K.M., Lin, N.-H., Wang, S.-H., Dokiya, Y., 2008. Rainwater chemistry at a high altitude station, Mt. Lulin, Taiwan: comparison with a background station, Mt. Fuji. Journal of Geophysical Research 113, D06305. http://dx.doi.org/10.1029/2006JD008248.